Hydrothermal synthesis, characterisation and growth mechanism of $Ni(SO_4)_{0.3}(OH)_{1.4}$ nanowires

Haoran Wang[1], Lei Wan[1], Yaqiong Chen[1], Wenbin Hu[1,2], Yida Deng[2]

[1]*School of Materials and Engineering, State Key Laboratory of Metal Matrix Composites, Shanghai Jiao Tong University, Shanghai 200240, People's Republic of China*
[2]*Key Laboratory of Advanced Ceramics and Machining Technology (Ministry of Education), and Tianjin Key Laboratory of Composite and Functional Materials, Tianjin University, Tianjin 300073, People's Republic of China*
E-mail: denyda@163.com

Published in Micro & Nano Letters; Received on 4th August 2014; Accepted on 8th July 2015

A report is presented on the facile fabrication of $Ni(SO_4)_{0.3}(OH)_{1.4}$ nanowires via the hydrothermal synthesis method. The outcome demonstrates that the existence of SO_4^{2-} and a comparatively lower pH are of great essence to form nanowires morphology rather than flake-like or amorphous ones. When the molar ratio of SO_4^{2-} to OH^- was 1:1, almost pure nanowires of diameter 20−30 nm and several micrometres long could be obtained. $Ni(SO_4)_{0.3}(OH)_{1.4}$ is actually a type of α-$Ni(OH)_2$. The growth mechanism of this hydroxyl-lacking hydroxide is discussed. The embedded SO_4^{2-} between $Ni(OH)_2$ layers can realise electrostatic equilibrium which may ensure an hcp crystal structure of $Ni(OH)_2$ having the trend to grow along the (001) direction. On the contrary, when SO_4^{2-} was superseded by other anions, the nanowires would progressively convert to nanosheets, accompanied by an α-phase to β-phase transformation.

1. Introduction: As a sort of well-known positive electrode active materials, $Ni(OH)_2$ has extensive use in nickel-based rechargeable alkaline batteries because of its high proton diffusion coefficient, power density, specific capacity and so on [1]. Meanwhile, it also has prospects to be exploited as fuel cells [2], adsorbents [3], supercapacitors [4, 5] and as precursors for NiO nanostructures [6], which attracts much attention from related researchers.

Until recently, investigations have been carried out to illuminate the growth mechanism of $Ni(OH)_2$ nanoparticles [7–9] due to the fact that the electrochemical performance of $Ni(OH)_2$ is strongly influenced by its size, structure and surface morphology [10]. Narrowing the size of $Ni(OH)_2$, could remarkably optimise its electrochemical performance, since a small crystalline size enjoys a high proton diffusion coefficient. It is well acknowledged that $Ni(OH)_2$ mainly takes on two forms that are α-type and β-type. In comparison with its more universally existing counterpart β-Ni$(OH)_2$ which is expressed as $Ni(OH)_2$, α-$Ni(OH)_2$ can be expressed as $Ni(OH)_{2-x}A^{n-}_{x/n} \cdot yH_2O$, where $Ni(OH)_{2-x}$ is the hydroxyl-lacking layers and A is the acid radical anions (for instance, NO_3^-, SO_4^{2-}, CO_3^{2-} and so forth) or water molecules. The value of x and y are generally 0.2−0.4 and 0.6−1.0, respectively, depending on the inserted anions and water molecules. In most cases, α-$Ni(OH)_2$ is unstable and is finally inclined to decay to β-$Ni(OH)_2$. In terms of SO_4^{2-} embedded α-$Ni(OH)_2$, an Ni$(OH)_{1.7}(SO_4)_{0.15}(H_2O)_{0.79}$ was discovered by P. Vishnu Kamath in 1997 [11]. Similar to this molecular formula, Yang and colleagues [12] synthesised $Ni(OH)_{1.66}(SO_4)_{0.17}(H_2O)_{0.29}$. Apart from the above-mentioned α-$Ni(OH)_2$, which looks a little complex in their stoichiometric expressions, $Ni(SO_4)_{0.3}(OH)_{1.4}$ is recently reported frequently by some groups [7, 12–15], with needle-like, belt-like and wire-like morphologies easily obtained via the hydrothermal synthesis method. What is more, their related properties and forming mechanism were also studied in several aspects, for example, pH value, reacting temperature and concentration of SO_4^{2-}. Owing to its sulphate-ion-abundant nature, after being treated under high temperature, it will decompose into NiO and SO_4^{2-}, while the remains of β-$Ni(OH)_2$ under the same condition can only contain NiO [15].

In spite of these above-mentioned successes, however, it remains a significant challenge to discover the relationship between the reaction condition and growth mechanism. It has been demonstrated that the concentration of OH^- ions can alter the ionic supersaturation, which may lead to variation in the morphology and crystal structure of the products. Besides, in the presence of SO_4^{2-} ions, $Ni(SO_4)_{0.3}(OH)_{1.4}$ nanowires can be successfully fabricated [7]. These research results shed light on the growth mechanism of Ni$(OH)_2$ nanoparticles. In this Letter, we focus on the effects of OH^- concentration and varieties of anions on the morphology of $Ni(OH)_2$. We focus on different factors that are in favour of the arising of nanowire $Ni(SO_4)_{0.3}(OH)_{1.4}$, including concentration of OH^-, the type of acid radical ions and reaction time. Through a facile hydrothermal route at 120°C, pure $Ni(SO_4)_{0.3}(OH)_{1.4}$ nanowires were prepared merely by NaOH and $NiSO_4$ without any surfactants or stabilisers, which profoundly simplifies the preparation process. Compared with former hydrothermal methods, the method devised in this Letter is a combination of all the merits of the former methods. The $Ni(SO_4)_{0.3}(OH)_{1.4}$ nanowires were prepared at a comparatively low temperature, with concise and inexpensive raw materials (which only require NaOH and $NiSO_4$). Besides, the high concentration of the mother solution and the time-dependence of the nanowires' morphologies make possible the potential of industrial manufacture. Drawing on experimental phenomena and previous reports, the growth mechanism of Ni$(SO_4)_{0.3}(OH)_{1.4}$ nanowires is also discussed. It is suggested that the existence of SO_4^{2-} without other acid radical anions and a low concentration of OH^- are two key factors to synthesise $Ni(SO_4)_{0.3}(OH)_{1.4}$ nanowires. In addition, the heat-treatment time also played an important role in their formation. Some related theories support the view that α-$Ni(OH)_2$ and intersecting nanowires network structures can advance the electrochemical properties [16, 17] which well match the as-synthesised $Ni(SO_4)_{0.3}(OH)_{1.4}$. Thus, it encourages us to conduct more investigations to explore relevant and potential electrochemical applications.

2. Experimental

2.1. Chemicals: Nickel sulphate hexahydrate ($NiSO_4 \cdot 6H_2O$), sodium hydroxide(NaOH), nickel chlorine hexahydrate ($NiCl_2 \cdot 6H_2O$), nickel nitrate hexahydrate ($Ni(NO_3)_2 \cdot 6H_2O$) and barium chloride ($BaCl_2$) which were purchased from the Sinopharm Chemical Reagent Co. Ltd were used without further

Table 1 Different $Ni(OH)_2$ morphology and phase obtained under different amounts of NaOH

Sample	NaOH, mmol	$NiSO_4$, mmol	Morphology
A	15	15	wire
B	23.5	15	wire and ribbon
C	24.6	15	sheet and ribbon
D	27	15	sheet

purification as they were all analytically pure. Deionised water prepared by an ultrapure water system (Millipore) was used throughout the experiment.

2.2. Fabrication of $Ni(SO_4)_{0.3}(OH)_{1.4}$ nanowires: In a typical procedure, 7.5 ml of NaOH (2 mol/l) was added dropwise to 52.5 ml of solution which contained 3.94 g of $NiSO_4{\cdot}6H_2O$. In this process, intense stirring was necessary. Followed with the addition of NaOH, viridian colloids were prepared. After being stirred for another 10 min, the precursor was transferred into a Teflon-lined stainless steel autoclave. The autoclave was sealed and maintained at 120°C for 24 h. After the reaction was complete, the autoclaves were cooled down naturally to room temperature (RT). The resulting green samples were washed several times with deionised water. Finally, the products were dried at 60°C for 24 h in vacuum atmosphere.

2.3. Study of effect of NaOH content on $Ni(OH)_2$ structure and morphology: Experiments were carried out under different NaOH contents, and representative results are listed in Table 1. All the experimental parameters had been converted to a molar concentration while the whole solution volume remained at 60 ml. Sample A just corresponded to the $Ni(SO_4)_{0.3}(OH)_{1.4}$ nanowires described above and the synthesis procedure of samples B, C and D were similar to A except for diverse NaOH dosages.

2.4. Influence of solution circumstance of anions on $Ni(OH)_2$ structure and morphology: To investigate the influence of different anions circumstance on the morphologies of $Ni(OH)_2$ under hydrothermal process, $NiCl_2$ and $Ni(NO_3)_2$ were applied (see Fig. 1). The same precursors were prepared by SO_4^{2-} as shown in Section 2.1. Then the as-synthesised precursor was divided into three parts. These sections were unwashed, washed three times and washed six times with $NiCl_2$ and $Ni(NO_3)_2$, respectively. As a result, the residual SO_4^{2-} were totally displaced by Cl^- or NO_3^-. To ensure no SO_4^{2-} remained, samples were detected by $BaCl_2$. Lastly, the precursors were transferred into a 100 ml Teflon-lined stainless steel autoclave (60% loading capacity) and maintained at 120°C for 24 h. The final samples were collected and treated as shown in Section 2.2.

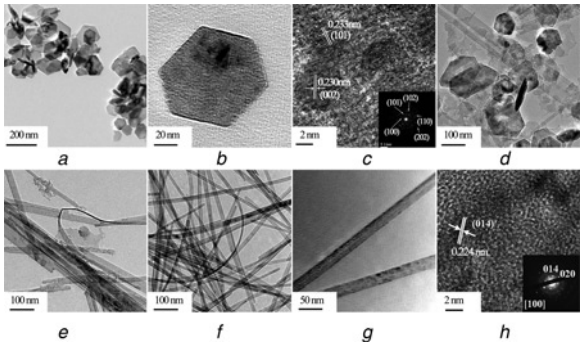

Figure 1 *TEM images of $Ni(OH)_2$ samples prepared with 27mmol NaOH (Fig. 1a); magnified image of single $Ni(OH)_2$ nanosheet (Fig. 1b); HRTEM image of $Ni(OH)_2$ nanosheets prepared with 27 mmol NaOH (Fig. 1c); (inset of Fig. 1c is corresponding SAED); TEM images of Ni $(OH)_2$ samples prepared with 24.6 mmol NaOH (Fig. 1d), with 23.5 mmol NaOH (Fig. 1e), and with 15mmol NaOH (Fig. 1f); magnified image of Ni $(OH)_2$ nanowires (Fig. 1g); HRTEM image of $Ni(OH)_2$ nanowires prepared with 15 mmol NaOH (Fig. 1h) (inset of Fig. 1h is corresponding SAED)*

2.5. Characterisation: Transmission electron microscopy (TEM) images and energy-dispersive spectroscopy (EDS) were obtained using a JEOL 2100F TEM with EDS. The TEM samples were obtained by dipping several drops of precursor on a carbon copper grid. X-ray diffraction (XRD) patterns were collected using a Rigaku D/2500 V/PC X-ray diffractometer. The Cu-Kα radiation ($\lambda = 1.5418$ Å) was at a scanning speed rate of 15°/min and the detective range from 10° to 90°. Fourier transform infrared spectra (FTIR) were recorded with the KBr pellet technique in the range of 4000–400 cm^{-1} on a model FTS135 infrared spectrophotometer (American BIO-RAD Company) operated at a resolution of 2 cm^{-1}. All the measurements were performed at RT.

3. Results and discussion

3.1. Morphologies and structures of $Ni(OH)_2$ obtained from different parameters: The TEM image in Fig. 1*a* reveals that the samples consist of a large number of nanosheets, which were prepared under higher NaOH concentrations. The nanosheets have hexagonal morphologies with sizes in the range of 40−80 nm. They showcase a high aspect ratio, for the thickness of these nanosheets is fairly thin, according to the low contrast in the graph. One of these nanosheets shows a regular hexagon with the adjacent edges forming angles of almost 120° (Fig. 1*b*). The lattice spacing of 0.233 and 0.230 nm in the high-resolution TEM (HRTEM) image (Fig. 1*c*) corresponds to the (101) and (002) spacing of the hexagonal $Ni(OH)_2$ phase. Several polycrystalline rings are shown in the inset of Fig. 1*c*, which can match up to (100), (101), (110), (102) and (202) of this phase correspondingly. When the content of NaOH decreased from 24.6 to 23.5 mmol, $Ni(OH)_2$ nanoribbons and nanowires started to generate. Typical TEM images are presented in Figs. 1*d* and *e*, which indicate that the samples are a mixture of nanosheets, nanoribbons and nanowires. The nanosheets in Fig. 1*d* have an irregular hexagonal morphology with sizes in the range of 60 −120 nm. It is worth mentioning that several ribbon-like nanoparticles running through the graph field have formed with a width of around 50 nm or so, which may lead to a trend that the $Ni(OH)_2$ will transform into another structure different from those nanosheets. It can be clearly seen that the samples in Fig. 1*e* are mainly composed of nanoribbons with few sheet-like products. The widths of some nanoribbons shrink significantly from their counterparts in Fig. 1*d*; thus they appear more like wires rather than ribbons. When the amount of NaOH descended to 15 mmol, it led to the formation of nanowires with widths of 20−30 nm as shown in Fig. 1*f*. The HRTEM image (Fig. 1*h*) presents the nanocrystalline lattice fringes with an interplanar distance of 0.224 nm, corresponding to the (014) interplanar distance of the wire-like $Ni(SO_4)_{0.3}(OH)_{1.4}$ phase. The weak, diffuse rings in the selected area electron diffraction (SAED) pattern (the inset of Fig. 1*h*) indicate that the samples are polycrystalline.

From the EDS [$Ni(OH)_2$ (see Fig. 2) nanowires prepared with 15 mmol NaOH], it can be seen that apart from carbon and copper that come from the copper–carbon grid used for TEM testing, the products are mainly composed of nickel, oxygen and no little sulphur.

Fig. 3 shows the XRD patterns of the $Ni(OH)_2$ samples A, B, C and D (listed in Table 1). The peak positions of the XRD patterns in samples A and B are in good agreement with that of the Ni $(SO_4)_{0.3}(OH)_{1.4}$ (JCPDS41–1424). This structure can just be categorised as a kind of α-$Ni(OH)_2$ with some portions of

doi: 10.1049/mnl.2015.0152

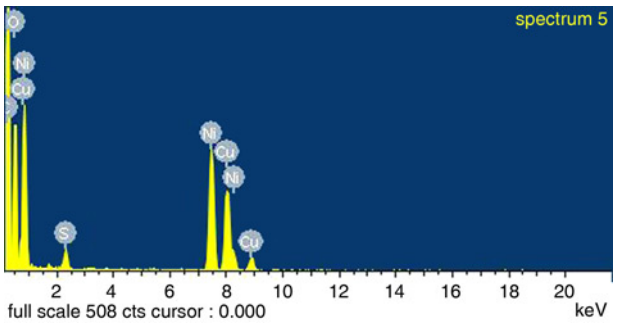

Figure 2 *EDS spectrum of $Ni(OH)_2$ obtained at n(NaOH) = 15 mmol*

hydroxyls being substituted by SO_4^{2-}. It is noted that the XRD pattern in sample A presents a higher peak intensity (I_{002}) than the peak intensity (I_{014}), which corresponds to the (002) and (014) crystal plane, respectively. On the other hand, the XRD pattern in sample B presents a totally opposite result: $I_{002} < I_{014}$. Considering that sample A mainly consists of $Ni(OH)_2$ nanowires and sample B is composed of nanowires and a few nanosheets, the changes in the relative intensity of diffraction show that the linear $Ni(OH)_2$ nanowires tend to grow along the (002) plane. When the component of $Ni(OH)_2$ nanowires declines with the increasing molar concentration of OH^-, the peak corresponding to the (002) plane recedes gradually. Moreover, for the $Ni(OH)_2$ samples C and D, the XRD patterns are matched with β-$Ni(OH)_2$ (JCPDS14–0117), which means further augmentation of OH^- bringing about a crystal form transformation from α-phase to β-phase, with their crystal forms corresponding to sheet-like and wire-like morphologies accordingly. The XRD pattern of sample C presents $I_{001} > I_{101}$ and sample D shows $I_{001} < I_{101}$. One can also come to the conclusion that OH^- can affect the trend of the plane growing. In summary, the crystal structure and morphologies of $Ni(OH)_2$ are closely related to the amount of OH^-. The molar ratio 1.6:1, $n(SO_4^{2-})$ compare with $n(OH^-)$, is a critical point. Beyond that point, the linear α-type nanowire starts to convert to its β-type counterpart.

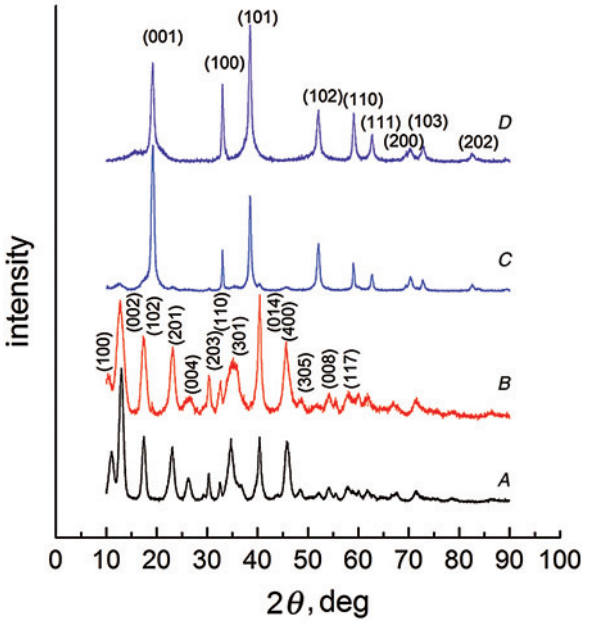

Figure 3 *XRD patterns of $Ni(OH)_2$ samples with different amounts of NaOH. A: 15 mmol; B: 23.5 mmol; C: 24.6 mmol; D: 27 mmol*

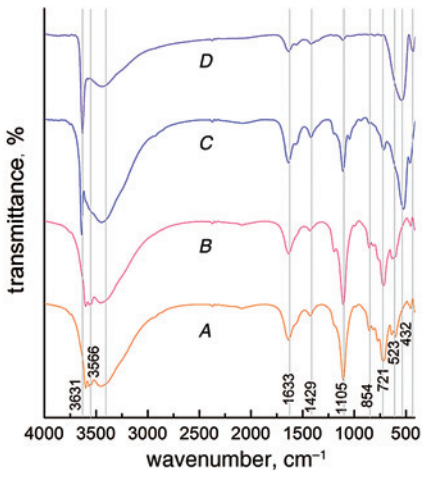

Figure 4 *FTIR spectra of $Ni(OH)_2$ samples with different amounts of NaOH. A: 15 mmol; B: 23.5 mmol; C: 24.6 mmol; D: 27 mmol*

The FTIR spectrum of samples A, B, C and D are shown in Fig. 4 The vibration bands in the FTIR spectra are labelled with vertical lines. The sharp valleys at ca. 3631 cm^{-1} in samples C and D are attributed to the ν_{OH-} (ν: stretching vibration) stretching of geminal free hydroxyl groups in β-$Ni(OH)_2$. Analogously, the broad valleys at ca. 3566 cm^{-1} in samples A and B are due to the ν_{OH} vibration of H-bonded water molecules embedded in the interlamellar space of the turbostratic structure of α-$Ni(OH)_2$. The valleys in the four samples at ca. 1633 cm^{-1} are characterised by the bending vibrational mode of the interlayer water molecules. The vibration at ca. 432 cm^{-1} can be due to metal–oxygen vibrations and metal–oxygen–hydrogen bending vibrations, which can be ascribed to Ni-OH in this system. The sharp valleys at ca. 1105 cm^{-1} in samples A, B and C are due to the ν_{HSO4} vibration of H-bonded SO_4^{2-} anions. The valleys at ca. 854 and 721 cm^{-1} in samples A and B can be assigned to the vibration of SO_4^{2-} [18–20]. Crucially, it is pointed out that the $\nu_{SO_4^{2-}}$ vibration can only be observed in $Ni(SO_4)_{0.3}(OH)_{1.4}$ nanowires, namely, the α-$Ni(OH)_2$.

Fig. 5 demonstrates the TEM images of $Ni(OH)_2$ obtained from various sorts of anions with different times. Identical with those from Fig. 1*f*, Figs. 5*a* and *d* reveal that the samples are completely made up of nanowires with 20−30 nm width, when the $Ni(OH)_2$

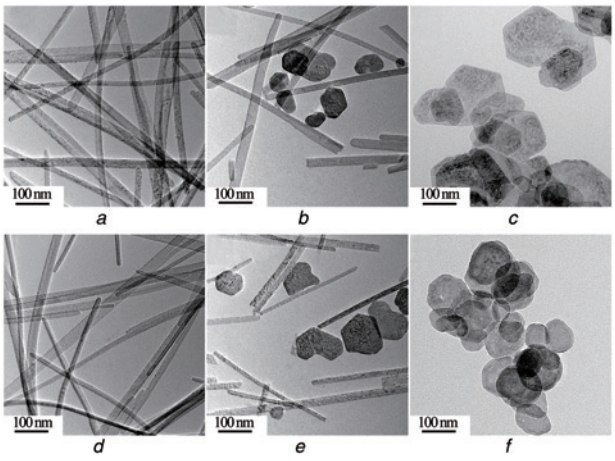

Figure 5 *TEM images of $Ni(OH)_2$ unwashed samples (Fig. 5a) and of $Ni(OH)_2$ samples washed by nickel chlorine three times (Fig. 5b) and six times (Fig. 5c) before hydrothermal reaction; Figs. 5d–f: counterparts compared with Figs. 1a–c, they were washed by nickel nitrate*

precursors were not rinsed with $NiCl_2$ or $Ni(NO_3)_2$. After the $Ni(OH)_2$ precursors were washed three times with $NiCl_2$ or $Ni(NO_3)_2$, however, the hydrothermal circumstance of the solutions were a mixture of SO_4^{2-} and Cl^- or NO_3^-, and a few sheet-like products emerged (Figs. 5*b* and *e*). Meanwhile, it is clear that the lengths of these nanowires shrink to a submicron order, which may be due to the impact of Cl^- and NO_3^-. When precursors contained just SO_4^{2-}, almost no nanowire would terminate within the visual field (Figs. 5*a* and *d*). After the $Ni(OH)_2$ precursors were washed six times with $NiCl_2$ or $Ni(NO_3)_2$ solution, the content of the remaining SO_4^{2-} can almost be neglected; under this circumstance, hexagonal nanosheets with sizes in the range of 40–80 nm were obtained after the hydrothermal treatment. From the above phenomena, it can be concluded that anions have a significant effect on the structure and morphology $Ni(OH)_2$. The existence of SO_4^{2-} is critical in producing wire-like structures, while the Cl^- and NO_3^- are beneficial to the formation of $Ni(OH)_2$ nanosheets.

3.2. Growth mechanism of $Ni(SO_4)_{0.3}(OH)_{1.4}$ nanowires: According to the above experimental results, the amount of NaOH and sorts of anios circumstance have played a critical role in synthesising different structures and morphologies of $Ni(OH)_2$ during the hydrothermal process. To explain the formation of different $Ni(OH)_2$ nanostructures, it is crucial to understand the $Ni(OH)_2$ crystallography structure. Generally speaking, $Ni(OH)_2$ has a hexagonal crystal structure which harbours an ABAB stacking sequence. The OH^- and Ni^{2+} layers stack alternatively along the *c*-axis (as shown in Fig. 6) and grow on the *XY*-plane. Between two adjacent OH^- planes, there exists octahedral voids that Ni^{2+} fills and this constitutes a $Ni(OH)_6$ octahedron [20]. Both α-phase and β-phase can be regarded as the accumulation of $Ni(OH)_6$ octahedrons. The difference is that for the α-phase $Ni(OH)_2$, the distance between OH^- layers is far larger than its counterpart because water molecules and other ions enter into the layers [21]; for instance, the sulphate ion.

In the hydrothermal process, one-dimensional or other nanostructures will be fabricated by controlling the reactant type, concentration, reaction time, temperature and so on [7, 20, 22]. In this Letter, we find out that a low NaOH concentration and a high-purity SO_4^{2-} environment are the key factors to form $Ni(SO_4)_{0.3}(OH)_{1.4}$ nanowires. The formation mechanism of the $Ni(SO_4)_{0.3}(OH)_{1.4}$ nanowires is proposed as follows (as shown in Fig. 7). When the concentration of NaOH in the system is low, it is beneficial for forming $Ni(OH)_{2-x}$ $(x>0)$ stacking layered structures, which allow H-bonded water molecules to embed in the layered space to be the so-called $[Ni(OH)_{2-x}(H_2O)_x]^{x+}$ (Fig. 7*a*). To keep the charge balance at equilibria, other anions are bonded to the Ni $(OH)_{2-x}$ layer through electron absorption. It has been demonstrated that various anions such as CO_3^{2-}, SO_4^{2-}, OH^-, F^-, Cl^-, Br^-, NO_3^- and CH_3COO^- are able to enter the interlayer of the $Ni(OH)_2$ and the relative affinity of the layer towards these anions possesses the following sequence: $CO_3^{2-} > SO_4^{2-} > OH^- > F^- > Cl^- > Br^- > NO_3^- > CH_3COO^-$ [23, 24]. Once these anions enter into the lattice, the distance between two neighbouring Ni^{2+} layers is broadened to 0.7–0.8 nm (Fig. 7*b*) because of the relatively large volume of anions [21]. On account of the favourable coordination between SO_4^{2-} and Ni(II) (Fig. 7*c*), a new stable layered structure comes into being. That is to say, in the stage of crystal growth, the electrostatic attraction between SO_4^{2-} and $Ni(OH)_2$ layers and the hydrogen bond between OH^- and the water molecules can prompt the $Ni(OH)_2$ to grow along the *c*-axial direction and to form stable $Ni(SO_4)_{0.3}(OH)_{1.4}$ nanowires (Fig. 7*d*).

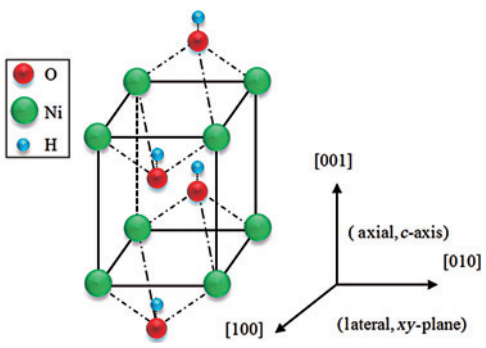

Figure 6 *Illustration of model for $Ni(OH)_2$ crystalline structure*

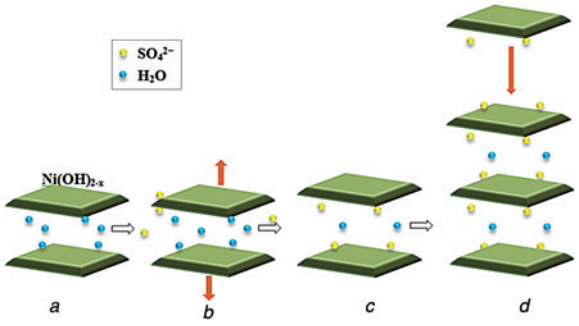

Figure 7 *Schematic illustration of model and growth mechanism for $Ni(OH)_2$ crystalline structure*
a Hydroxyl-laced $Ni(OH)_2$
b Elongation of *c*-axis
c Insertion of SO_4^{2-}
d Formation of $Ni(SO_4)_{0.3}(OH)_{1.4}$

To further support our presupposition, several samples that experienced different heat treatment durations have been considered. Their process parameters were the same as the fabrication of Ni $(SO_4)_{0.3}(OH)_{1.4}$. Figs. 8*a–d* show samples treated by 0 (namely untreated), 2, 4 and 15 h and A, B, C and D in Fig. 8*e* are their XRD patterns, respectively. When no heat treatment was introduced, as can be seen from Fig. 8*a*, the sample's morphology is a far cry from its 24 h heat-treated counterpart in Fig. 1*f*, which is a cotton-like precipitation. After 2 h (Fig. 8*b*), not much has changed. However, dispersibility of the agglomeration is better, which may herald the beginning of some alterations. Both XRD patterns of Figs. 8*a* and *b* can correspond to β-$Ni(OH)_2$ (JCPDS14–0117). Owing to their insufficient heat treatment intervals, the peaks of them are both broader than those in C and D of Fig. 3. With SO_4^{2-} starting to enter between OH^- layers, wire-like nanoparticles can be observed in Fig. 8*c*, and the corresponding XRD pattern (C of Fig. 8*e*) turns out to be $Ni(SO_4)_{0.3}(OH)_{1.4}$(JCPDS41–1424). The crystallisation process is full blown after 15 h of heat treatment. In this case, the XRD peaks of this sample, as shown in D of Fig. 8*e*, are sharper than their 4 h-treated equivalent. Most importantly, the lengths of the nanowires in Fig. 8*d* are much longer than those in Fig. 8*c*, showing almost no difference from those in Fig. 1*f*. Considering the fact that the SO_4^{2-} will enter in the *c*-axis direction, the elongation of nanowires is indicative of sufficient insertion of SO_4^{2-}.

On the other hand, distinct from SO_4^{2-}, the Cl^- or NO_3^- ions cannot be stably embedded between the $Ni(OH)_2$ layers. When the SO_4^{2-} anions in the solutions were partially or completely replaced by the Cl^- or NO_3^- anions, the $Ni(OH)_2$ crystal tends to grow along the lateral direction and finally form β-$Ni(OH)_2$ nanosheets. Of course, $Ni(SO_4)_{0.3}(OH)_{1.4}$ nanowires cannot form under a high OH^- concentration condition either. First, the Ni $(OH)_2$ structure whose hydroxyls are sufficient has been stabilised, thus there is no place for redundant anions to enter. Secondly, the electrostatic repulsion between the OH^- layers is strong under this circumstance. This hinders further growing or stacking along the (001) direction. Therefore, the crystal is inclined to form

doi: 10.1049/mnl.2015.0152

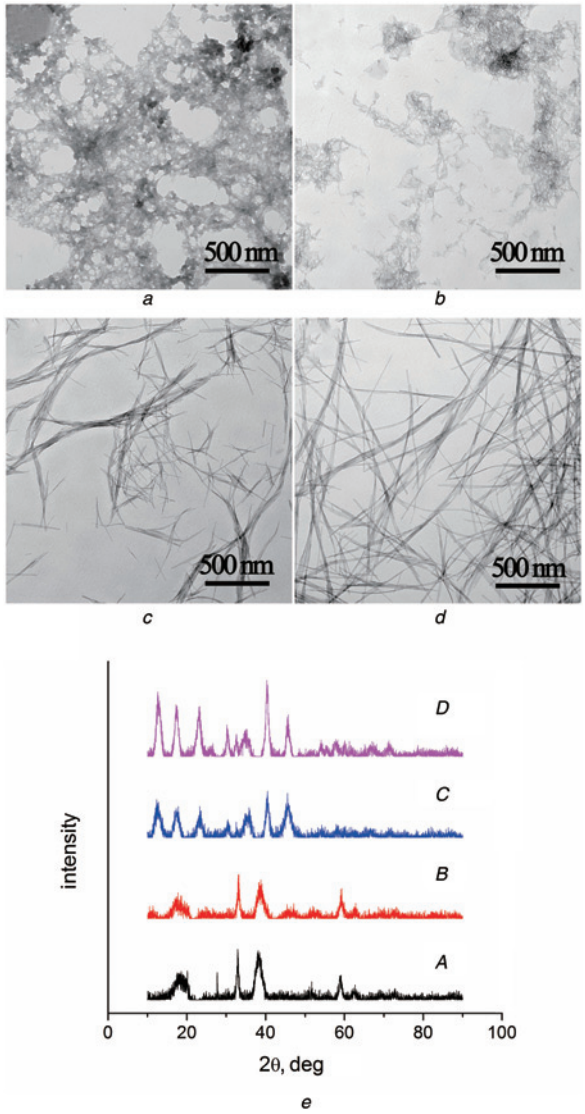

Figure 8 *TEM images of α-Ni(OH)$_2$ heat treated under different periods. Among them, the periods are: primitive untreated sample (Fig. 8a), 2 h (Fig. 8b), 4 h (Fig. 8c), 15 h (Fig. 8d); in Fig. 8e A, B, C and D are XRD patterns of Figs. 8a–d, correspondingly*

along these easier growing directions, namely the (100) or (010) ones. If we continue increasing the pH value, the discrepancy among various crystal faces is further narrowed. At this moment, globular nanoparticles are emerging which conform to former researches [7].

4. Conclusion: In summary, $Ni(SO_4)_{0.3}(OH)_{1.4}$ nanowires were synthesised using a hydrothermal method by controlling the content of NaOH and the varieties of anions in the hydrothermal treatment process. When the content of NaOH was <15 mmol and the anions of the solution were SO_4^{2-} ions, the Ni $(SO_4)_{0.3}(OH)_{1.4}$ nanowires with an average diameter of about 20 −30 nm and length of about several micrometres were obtained. This reveals that the low content of NaOH and the pure SO_4^{2-} environment in the hydrothermal treatment are the key factors for synthesising $Ni(SO_4)_{0.3}(OH)_{1.4}$ nanowires. The low NaOH concentration and high purity of the SO_4^{2-} solution system promote the growth of nanocrystals along the (001) direction and the formation of $Ni(SO_4)_{0.3}(OH)_{1.4}$ nanowires. This phenomenon can be ascribed to the favourable bond between SO_4^{2-} and Ni^{2+} and the OH^- shortage condition. On the basis of these α-Ni(OH)$_2$ nanowires, further studies can be conducted to investigate their properties and potential applications.

5. Acknowledgments: This work was supported by the National Science Fund for Distinguished Young Scholars (no. 51125016), and by the National Natural Science Foundation of China (no. 51001075, no. 51371119).

6 References

[1] Chen J., D.H.B., Dou, S.X., Liu H.K.: 'Nickel hydroxide as an active material for the positive electrode in rechargeable alkaline batteries', *J. Electrochem. Soc.*, 1999, **146**, (10), pp. 3606–3612

[2] Choi B., Lee S., Fushimi C., Tsutsumi A.: 'Development of NiMH-based fuel cell/battery (FCB) system: characterization of Ni $(OH)_2/MnO_2$ positive electrode for FCB', *J. Power Sources*, 2009, **194**, (2), pp. 1150–1155

[3] Cheng B., Le Y., Cai W., Yu J.: 'Synthesis of hierarchical $Ni(OH)_2$ and NiO nanosheets and their adsorption kinetics and isotherms to Congo red in water', *J. Hazard. Mater.*, 2011, **185**, (2–3), pp. 889–897

[4] Kong L.-B., Lang J.-W., Liu M., Luo Y.-C., Kang L.: 'Facile approach to prepare loose-packed cobalt hydroxide nano-flakes materials for electrochemical capacitors', *J. Power Sources*, 2009, **194**, (2), pp. 1194–1201

[5] Cao C.Y., Guo W., Cui Z-M., Song W-G., Cai W.: 'Microwave-assisted gas/liquid interfacial synthesis of flowerlike NiO hollow nanosphere precursors and their application as supercapacitor electrodes', *J. Mater. Chem.*, 2011, **21**, pp. 3204–3209

[6] Zhu Z., Wei N., Liu H., He Z.: 'Microwave-assisted hydrothermal synthesis of $Ni(OH)_2$ architectures and their *in situ* thermal conversion to NiO', *Adv. Powder Technol.*, 2011, **22**, (3), pp. 422–426

[7] Sun D., Zhang J., Ren H., Cui Z., Sun D.: 'Influence of OH^- and SO_4^{2-} anions on morphologies of the nanosized nickel hydroxide', *J. Phys. Chem. C*, 2010, **114**, (28), pp. 12110–12116

[8] Khan Y., Durrani S.K., Mehmood M., Jan A., Abbasi M.A.: 'pH-dependant structural and morphology evolution of $Ni(OH)_2$ nanostructures and their morphology retention upon thermal annealing to NiO', *Mater. Chem. Phys.*, 2011, **130**, (3), pp. 1169–1174

[9] Liang H., Liu L., Yang Z., Yang Y.: 'Hydrothermal synthesis of ultralong single-crystalline α-$Ni(OH)_2$ nanobelts and corresponding porous NiO nanobelts', *Cryst. Res. Technol.*, 2010, **45**, (6), pp. 661–666

[10] Reisner D.E., Salkind A.J., Strutt P.R., Xiao T.D.: 'Nickel hydroxide and other nanophase cathode materials for rechargeable batteries', *J. Power Sources*, 1997, **65**, (1–2), pp. 231–233

[11] Kamath P.V., Annal Therese G.H., Gopalakrishnan J.: 'On the existence of hydrotalcite-like phases in the absence of trivalent cations', *J. Solid State Chem.*, 1997, **128**, (1), pp. 38–41

[12] Yang D., Wang R., Zhang J., Liu Z.: 'Synthesis of nickel hydroxide nanoribbons with a new phase: a solution chemistry approach', *J. Phys. Chem. B*, 2004, **108**, (23), pp. 7531–7533

[13] Ocaña M.: 'Preparation and characterization of uniform needle-like particles of nickel basic sulfate', *J. Colloid Interface Sci.*, 2000, **228**, (2), pp. 259–262

[14] Dong L., Chu Y., Sun W.: 'Controllable synthesis of nickel hydroxide and porous nickel oxide nanostructures with different morphologies', *Chem., Eur. J.*, 2008, **14**, (16), pp. 5064–5072

[15] Yiwen T., Zhiyong J., Yun J., Luying L., Jianbo W.: 'Simple template-free solution route for the synthesis of $Ni(SO_4)_{0.3}$ $(OH)_{1.4}$ nanobelts and their thermal degradation', *Nanotechnology*, 2006, **17**, (22), p. 5686

[16] Faure C., Delmas C., Fouassier M.: 'Characterization of a turbostratic α-nickel hydroxide quantitatively obtained from an $NiSO_4$ solution', *J. Power Sources*, 1991, **35**, (3), pp. 279–290

[17] Rajamathi M., Vishnu Kamath P.: 'On the relationship between α-nickel hydroxide and the basic salts of nickel', *J. Power Sources*, 1998, **70**, (1), pp. 118–121

[18] Liu B.-H., Yu S.-H., Chen S.-F., Wu C.-Y.: 'Hexamethylenetetramine directed synthesis and properties of a new family of α-nickel hydroxide organic−inorganic hybrid materials with high chemical stability', *J. Phys. Chem. B*, 2006, **110**, (9), pp. 4039–4046

[19] Ramesh T.N., Kamath P.V.: 'Synthesis of nickel hydroxide: effect of precipitation conditions on phase selectivity and structural disorder', *J. Power Sources*, 2006, **156**, (2), pp. 655–661

[20] Sarkar S., Pradhan M., Sinha A.K., Basu M., Negishi Y., Pal T.: 'An aminolytic approach toward hierarchical β-Ni(OH)2 nanoporous

architectures: a bimodal forum for photocatalytic and surface-enhanced Raman scattering activity', *Inorg. Chem.*, 2010, **49**, (19), pp. 8813–8827

[21] Köhler U., Antonius C., Bäuerlein P.: 'Advances in alkaline batteries', *J. Power Sources*, 2004, **127**, (1–2), pp. 45–52

[22] Matsui K., Kyotani T., Tomita A.: 'Hydrothermal synthesis of single-crystal $Ni(OH)_2$ nanorods in a carbon-coated anodic alumina film', *Adv. Mater.*, 2002, **14**, (17), pp. 1216–1219

[23] Qi Y., Qi H., Li J., Lu C.: 'Synthesis, microstructures and UV–vis absorption properties of β-$Ni(OH)_2$ nanoplates and NiO nanostructures', *J. Cryst. Growth*, 2008, **310**, (18), pp. 4221–4225

[24] Li H., Ma J., Evans D.G., Zhou T., Li F., Duan X.: 'Molecular dynamics modeling of the structures and binding energies of α-nickel hydroxides and nickel–aluminum layered double hydroxides containing various interlayer guest anions', *Chem. Mater.*, 2006, **18**, (18), pp. 4405–4414

doi: 10.1049/mnl.2015.0152